ACS Energy LETTERS

Cite This: ACS Energy Lett. 2019, 4, 1549−1555

http://pubs.acs.org/journal/aelccp

LETTER

Selective Alcohol on Dark Cathodes by Photoelectrochemical CO_2 Valorization and Their In Situ Characterization

Myung Jong Kang,[⊥,‡,†] Chang Woo Kim,[∥,†] Amol U. Pawar,[⊥] Hyun Gil Cha,[‡] Sohyun Ji,[⊥] Wen-Bin Cai,[§] and Young Soo Kang*[,⊥]

[⊥]Korea Center for Artificial Photosynthesis and Department of Chemistry, Sogang University, Seoul 04107, Republic of Korea

[∥]Department of Graphic Arts Information Engineering, College of Engineering, Pukyong National University, Busan 48513, Republic of Korea

[‡]Center for Bio-based Chemistry, Korea Research Institute of Chemical Technology (KRICT), Ulsan 44429, Republic of Korea

[§]Department of Chemistry, Fudan University, Shanghai 200433, People's Republic of China

Supporting Information

ABSTRACT: Valorization of CO_2 into chemical fuel by photoelectrochemical CO_2 reduction competes with hydrogen evolution reaction. Considering that CO_2 reduction reaction (CO_2RR) occurs on the interface of the cathode in artificial photosynthesis, selectivity and faradaic efficiency depend on the performance of the cathode itself. Herein, we report a Nafion-coated TiO_2 dark cathode to produce alcohol as a selective liquid product from CO_2RR. The mechanism for selective alcohol production is investigated by in situ extended X-ray absorption fine structure and in situ electron paramagnetic resonance spectroscopy measurement for the intermediate CO_2 radical detection. The Nafion functional layer on the TiO_2 dark electrode suppresses the dimerization of monocarbon radical intermediates due to the efficient one-pot reactions of proton-coupled multiple electron transfer. As a result, the dimerization of monocarbon radical intermediates is suppressed due to decreased lifetime of the intermediate, facilitating the exclusive methanol production.

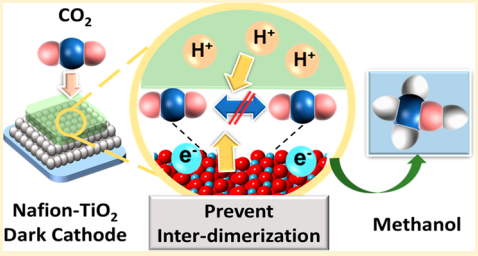

The rising CO_2 concentration in the global atmosphere and utilization of renewable energy are some of the most urgent challenges, which lead to replacement of fossil fuel-based energy to ecofriendly energy sources such as solar, wind, biomass, etc.[1,2] The artificial path of CO_2 valorization, which is CO_2 conversion to value-added products, is powered by solar light energy and a transferred proton by the water medium. Called artificial photosynthesis, a series of mimicking processes of natural photosynthesis produce a wide range of reduced carbon compounds, leading to a promising technique for sustainable energy generation.[3−5] At first, research on artificial photosynthesis started with that on hydrogen generation by a solar light-driven water splitting reaction.[6,7] Hydrogen production driven by solar light energy has been dramatically researched in the viewpoint of product efficiency through favorable kinetics and thermodynamically stable pathways.[8] However, concern over the low energy density of hydrogen gas as an energy source has facilitated the necessity of hydrocarbon production for highly dense energy sources.[9,10] As such, liquid fuels derived from CO_2 by solar light energy have been regarded as an emerging ecofriendly energy source with high energy density in terms of sustainable solar energy utilization and recycling of environmental destructive CO_2 gas.[11−13]

Thermodynamically stable CO_2 molecules can be evolved to a wide range of C_1 and C_2 hydrocarbon molecules like carbon monoxide (CO), formic acid (HCOOH), formaldehyde (HCHO), methane (CH_4), methanol (CH_3OH), ethylene (C_2H_4), and ethanol (CH_3CH_2OH). Especially, alcohols derived from CO_2 molecules have a considerable importance from a scientific and industrial aspect because of utilization of alcohol as a fuel source for internal combustion engines and also as the anode fuel of direct methanol fuel cells that inherently cut off the emission of CO, hydrocarbons, and nitrogen oxides by incomplete combustion.[14−16] To date, possible evolution paths have been suggested via photoelectrochemical (PEC), electrochemical (EC), photochemical (PC), etc. in recent research articles.[17,18] In addition, thermodynamic and kinetic parameters of the rate-determining step for final products have been explored based on

Received: April 29, 2019
Accepted: June 10, 2019
Published: June 10, 2019

DOI: 10.1021/acsenergylett.9b00927
ACS Energy Lett. 2019, 4, 1549−1555

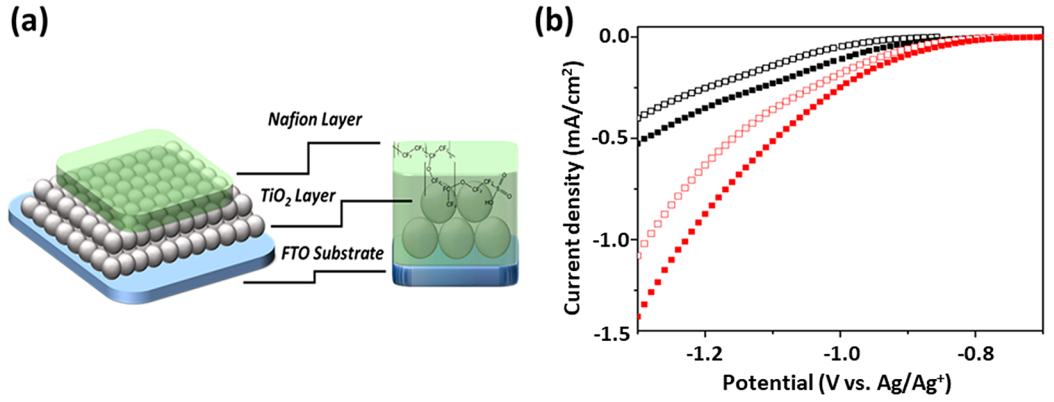

Figure 1. (a) Schematic illustration of a layer-by-layer Nf-TiO_2 dark cathode and (b) LSV curve of a TiO_2 dark cathode under N_2 gas flow (black □) and under $^{13}CO_2$ gas flow (black ■) and a Nf-TiO_2 dark cathode under N_2 gas flow (red □) and under $^{13}CO_2$ gas flow (red ■).

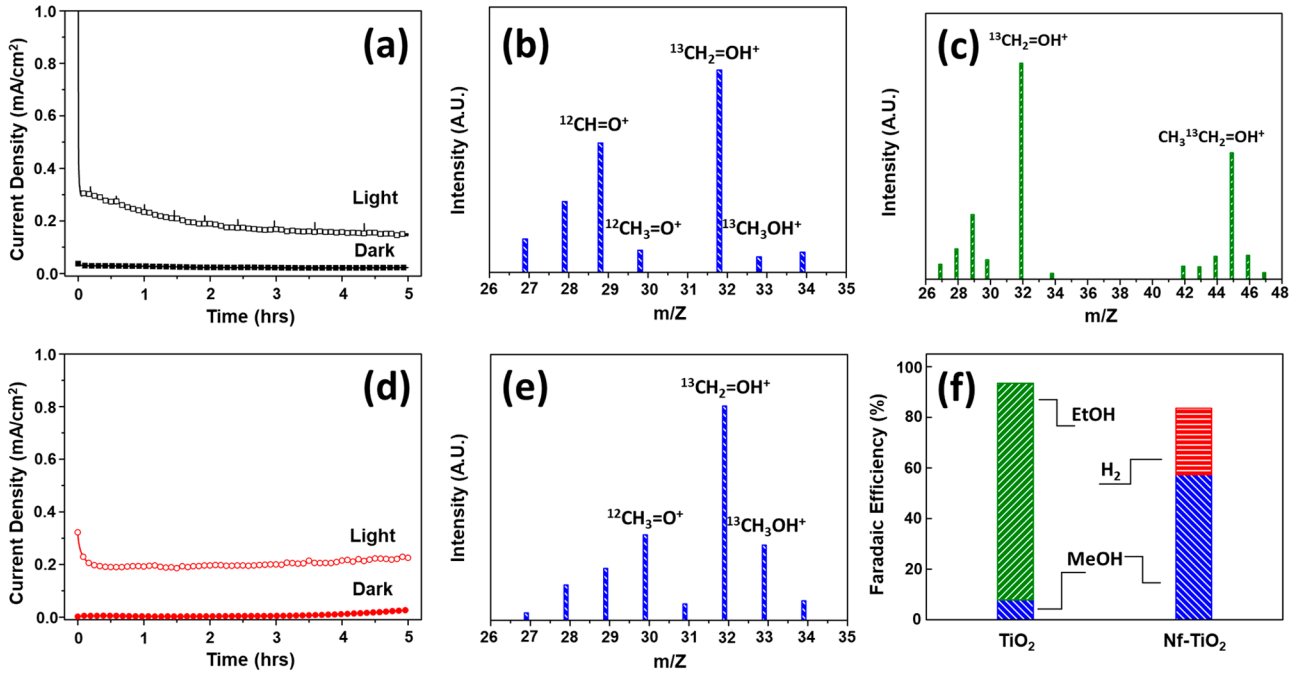

Figure 2. (a) $J-t$ curves of the TiO_2 dark cathode and GC-MS spectra of (b) methanol and (c) ethanol evolved by $^{13}CO_2$ on a TiO_2 dark cathode as a liquid product. (d) $J-t$ curves of a Nf-TiO_2 dark cathode and (e) GC-MS spectrum of methanol evolved by $^{13}CO_2$ on a Nf-TiO_2 dark cathode as a liquid product. (f) Faradaic efficiency of overall products on TiO_2 and Nf-TiO_2 dark cathodes.

computational DFT calculations.[19,20] Though a wide range of products evolved from CO_2 molecules has been revealed, the product selectivity has yet remained as an urgent challenging task because of the lack of fundamental understanding of it. Besides, subsidiary evolution of hydrogen gas has been unfavorably performed to deplete overall product efficiency as a competitive reaction during the conversion process of CO_2 reduction.

The introduction of aqueous electrolyte in a solar light-driven CO_2 reduction system is accompanied by proton reduction reaction, which leads to favorably produce hydrogen gas as the competitively parallel reaction.[21] Correspondingly, the introduction of an nonaqueous aprotic solvent has an eight times higher CO_2 solubility than aqueous media at atmospheric pressure and room temperature and is expected to contribute to higher mass transport of the CO_2 molecule. The PEC CO_2 reduction system with an nonaqueous aprotic solvent is expected to offer more chances for the CO_2 molecule to reduce on a cathodic electrode surface and inhibit hydrogen gas production as well.[22]

Herein, the present work reports a PEC CO_2 reduction system for alcohol selectivity, which is introduced with acetonitrile (ACN) for high CO_2 solubility and a Nafion layer for fast proton transport.[23] A (040) crystal facet-exposed $BiVO_4$ film ((040)-BVO) is used as the photoanode for high solar light absorption and efficient charge separation.[24,25] A Nafion-functionalized TiO_2 dark cathode is used to contribute reaction sites for efficient CO_2 adsorption.[26] Tetra-ethyl-ammonium perchlorate (TEAP) in ACN−water mixture reaction media is used for increasing CO_2 solubility.[27] As a proton source, some of the water serves to produce liquid hydrocarbons and inhibit CO evolution.[28] A Nafion membrane is adopted to separate the anode and cathode compartments to prevent production of hydrocarbons from reoxidation, and it also offers proton transport through each compartment. With an in situ extended X-ray absorption fine structure (EXAFS)

DOI: 10.1021/acsenergylett.9b00927
ACS Energy Lett. 2019, 4, 1549−1555

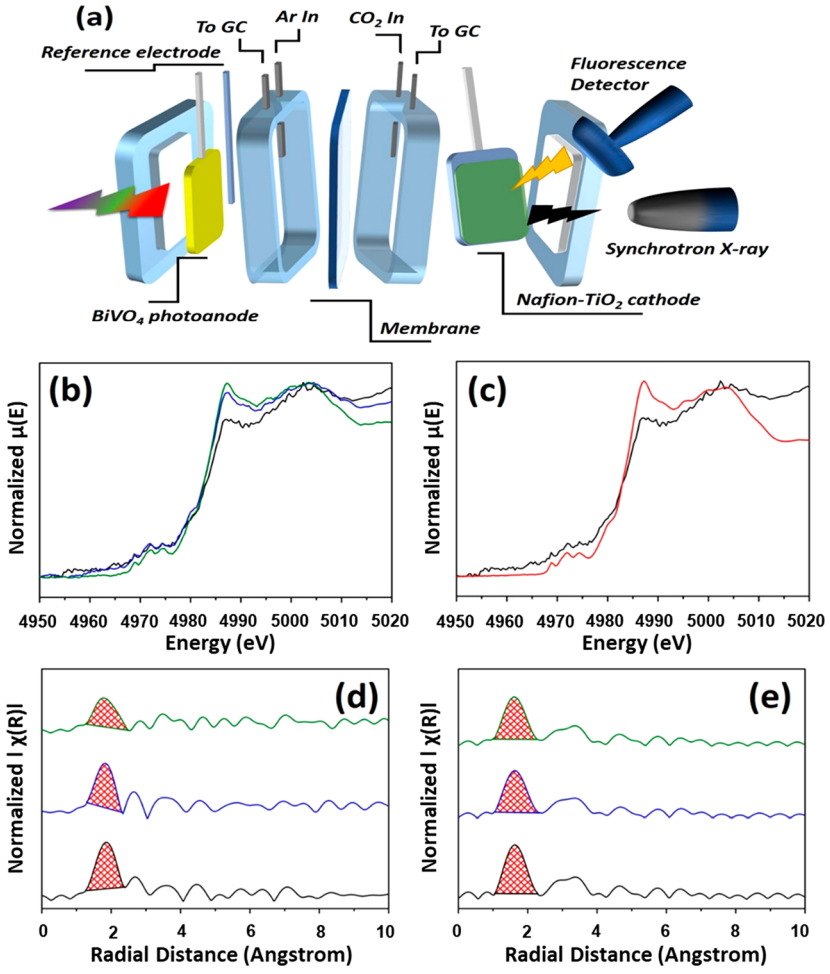

Figure 3. (a) Schematic drawings of in situ EXAFS measurement. (b) XAFS spectra on the TiO_2 dark cathode (black: cathode immersed into electrolyte; blue: under CO_2 purging flow; green: during PEC CO_2RR). (c) XAFS spectra on TiO_2 (black) and the Nf-TiO_2 (red) dark cathode during PEC CO_2RR. Refined EXAFS spectra for (d) TiO_2 and the (e) Nf-TiO_2 dark cathode (black: cathode immersed into electrolyte; blue: under CO_2 purging flow; green: during PEC CO_2RR).

analysis, in situ electron paramagnetic resonance spectroscopy (EPR), and ^{13}C-labeled gas chromatography with mass spectrometer (GC-MS) analysis, the mechanism for C_1 and C_2 alcohol with high liquid product selectivity in the present system is investigated and suggested.

As motivation with the utilization of a dark cathode for Cu_2O stability by Prof. Gong,[29] the Nafion functional layered TiO_2 electrode is introduced to unravel the path of alcohol evolution in the current work. The Nafion-coated TiO_2 dark cathode (Nf-TiO_2) is prepared by a facile doctor blading method on a fluorine-doped tin oxide (FTO) substrate, and spin coating of Nafion solution follows on a TiO_2 electrode (see the details in the Experimental Section of the Supporting Information). The Nafion functional layer is positioned on the surface of TiO_2 nanoparticles, as shown in the schematic structure of the Nf-TiO_2 dark cathode in Figure 1a. As expected, the crystal structure of pristine anatase TiO_2 (JCPDS #21-1272) was formed in the Nf-TiO_2 dark cathode because commercial TiO_2 paste was loaded on FTO even after Nafion coating (Figure S1).

The electrochemical properties of both TiO_2 and Nf-TiO_2 dark cathodes were evaluated by linear sweep voltammetry (LSV) curves depending on the N_2 and $^{13}CO_2$ purging flow (Figure 1b). The onset potentials (V_{onset}) of TiO_2 and Nf-TiO_2 under N_2 purging flow are −0.857 and −0.753 V vs Ag/Ag$^+$, respectively. Under CO_2 purging flow, the V_{onset} values of TiO_2 and Nf-TiO_2 are changed to −0.773 and −0.701 V vs Ag/Ag$^+$, respectively. The V_{onset} under a N_2 purged atmosphere stands for the initiation of hydrogen evolution by proton reduction on the surface of the cathode, while the V_{onset} under a $^{13}CO_2$ purged atmosphere stands for the initiation of CO_2 reduction reaction (CO_2RR) on the surface of the cathode. As such, the driving force for the increasing current density and the decreased V_{onset} of −0.701 V in the Nf-TiO_2 dark cathode should be derived from the Nafion layer coating. Compared with those of the TiO_2 dark cathode, the increased proton concentration in the catholyte, especially around the cathode surface because of the contribution of a surface-coated Nafion layer, induces a fast charge transfer on the cathode surface[30,31] and results in a high current density and lower V_{onset}.

Together with the (040)-BVO photoanode for proton generation in the PEC CO_2 reduction system (Figure S2), favorable CO_2 reduction conditions are offered on the dark cathode by the Nafion functional layer as a proton transfer medium to the cathode surface and as a CO_2 molecule absorber as well. On the basis of the above LSV results of both dark cathodes, the applied bias potential during PEC CO_2 reduction is determined to be −0.8 V vs Ag/Ag$^+$, which can minimize hydrogen evolution reaction as the side reaction of PEC CO_2RR.[32]

DOI: 10.1021/acsenergylett.9b00927
ACS Energy Lett. 2019, 4, 1549−1555

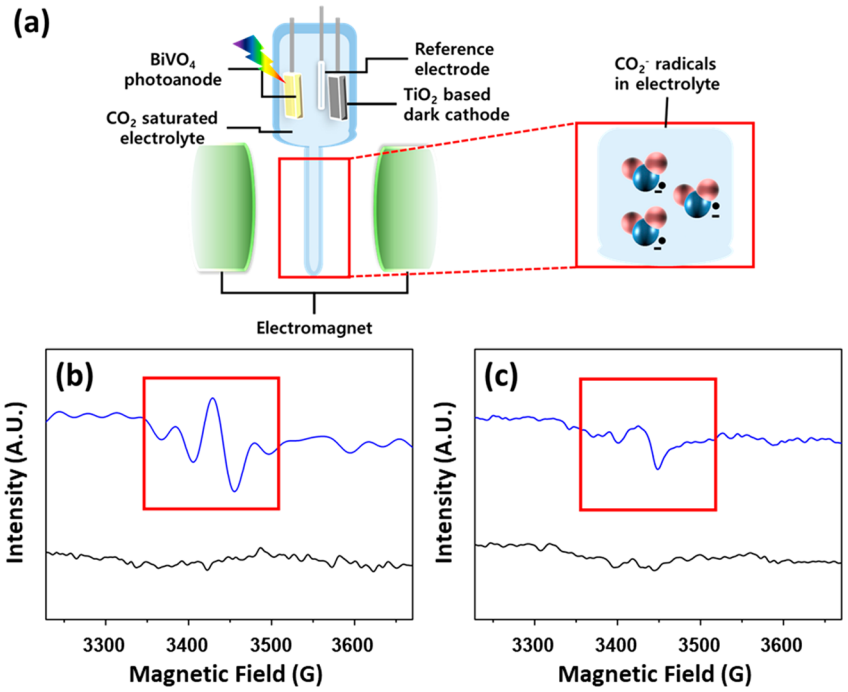

Figure 4. (a) Schematic illustration of in situ EPR measurement during PEC CO_2RR. EPR spectrum on a (b) TiO_2 dark cathode and (c) Nf-TiO_2 dark cathode (black: CO_2 purging into electrolyte; blue: during PEC CO_2RR, PBN was used as the trapping agent).

Both TiO_2 and Nf-TiO_2 dark cathodes were compared for PEC CO_2 reduction performances, as shown in Figure 2a,d. A −0.8 V vs Ag/Ag^+ external bias was applied to the (040)-BVO photoanode, and the chronoamperometry curves ($J-t$ curves) of both dark cathodes were monitored depending on illumination-on/off for CO_2RR. Under the illumination-off condition, the average current density was determined to be 0.02 mA cm^{-2} for both dark cathodes. The average current density of both dark cathodes was monitored as 0.23 mA cm^{-2} under illumination on the (040)-BVO photoanode. Strikingly, note that the current density shows negligible change between both dark cathodes. It indicates that mass transfer on the Nf-TiO_2 dark cathode was not disturbed by the Nafion layer and resulted in favorable electron and proton transfer on the catholyte. Liquid products on both dark cathodes after CO_2RR for 5 h were identified by nuclear magnetic resonance (NMR) quantification with standard calibration curves of ethanol and methanol, which have a nglet at 3.3 ppm and quartet at 3.6 ppm, respectively (Figure S3). The calculated amountsof methanol were 0.071 and 0.6 mM with TiO_2 and the Nf-TiO_2 dark cathode, respectively. Only the TiO_2 dark cathode produced 0.38 mM of ethanol, while Nf-TiO_2 converted CO_2 into methanol as unique liquid products (Figure S4). To clarify the origin of CO_2 reduction products, a ^{13}C-labeled study was performed with purging $^{13}CO_2$ during CO_2RR. Evolved alcohol from $^{13}CO_2$ gas like methanol and ethanol was clarified by ^{13}C-labeled $^{13}CO_2$ GC-MS analysis (Figure 2). The methanol produced by reduction of ^{13}C-labeled $^{13}CO_2$ showed its fingerprint peak of the $^{13}CH_2{=}OH^+$ ion at an m/z value of 32 (Figure 2b), and ethanol showed its fingerprint peak of the $CH_3{}^{13}CH_2{=}OH^+$ ion at an m/z value of 45 (Figure 2c), which was derived from ethanol produced by dimerization of CO_2 reduction intermediates during CO_2RR. The m/z values of the produced fingerprint peaks of ions for both methanol and ethanol are in good accordance with previously reported m/z values of commercial methanol and ethanol.[33] Evolved liquid products on the TiO_2 dark cathode were apparently confirmed as ^{13}C alcohol, which was mixed with ethanol as a major product and methanol as a minor product. Interestingly, the liquid product on the Nf-TiO_2 dark cathode was confirmed to be methanol as a major product that originated from ^{13}C CO_2 molecules. The Nf-TiO_2 system produced only methanol as a CO_2 reduction product, which was confirmed by the fingerprint peak of the $^{13}CH_2{=}OH^+$ ion at an m/z value of 32 (Figure 2e). Other gaseous products were also measured during reaction with the in situ GC system, and no gaseous product such as hydrogen by proton reduction reaction was produced on the TiO_2 dark cathode, as expected, to determine an anodic potential of 0.8 mV in LSV monitoring. However, on the Nf-TiO_2 dark cathode, hydrogen was detected as a gaseous product, which is explained with the following in situ EPR monitoring (Figure 4). On the basis of $J-t$ curve and product analyses results, the faradaic efficiency of each product is presented in Figure 2f. The calculated solar to liquid fuel efficiencies upon introducing TiO_2 and Nf-TiO_2 dark cathodes were 1.06 and 0.81%, respectively.

To investigate hydrocarbons from the PEC CO_2RR pathway using TiO_2 and Nf-TiO_2 dark cathodes, in situ EXAFS analysis and in situ EPR analysis were monitored. As shown in the schematic drawing of the in situ EXAFS system, the X-ray absorption fine structure (XAFS) spectrum of the TiO_2 dark cathode is shown in Figure 3. With the TiO_2 dark cathode immersed in electrolyte, the ΔE_0 was 21.2 eV, which has a Ti^{3+} and Ti^{4+} mixed state. CO_2 molecules purged into the electrolyte solution hold the oxidation state of Ti to the Ti^{3+}/Ti^{4+} mixed state as well. Interestingly, the Ti^{3+} oxidation state is formed only on the Ti surface during PEC CO_2RR. During CO_2RR, the ΔE_0 value changes to a ΔE_0 of 20.2 eV, which indicates the Ti^{3+} state, because of the higher electron density of Ti in the TiO_2 dark cathode due to electrons transported from the (040)-BVO photoanode. This tendency is also in good accordance with the Nf-TiO_2 dark cathode.

DOI: 10.1021/acsenergylett.9b00927
ACS Energy Lett. 2019, 4, 1549−1555

Scheme 1. Suggested C_1 (upper pathway) and C_2 (lower pathway) Alcohol Evolution Mechanism on TiO_2 and Nf-TiO_2 Dark Cathodes

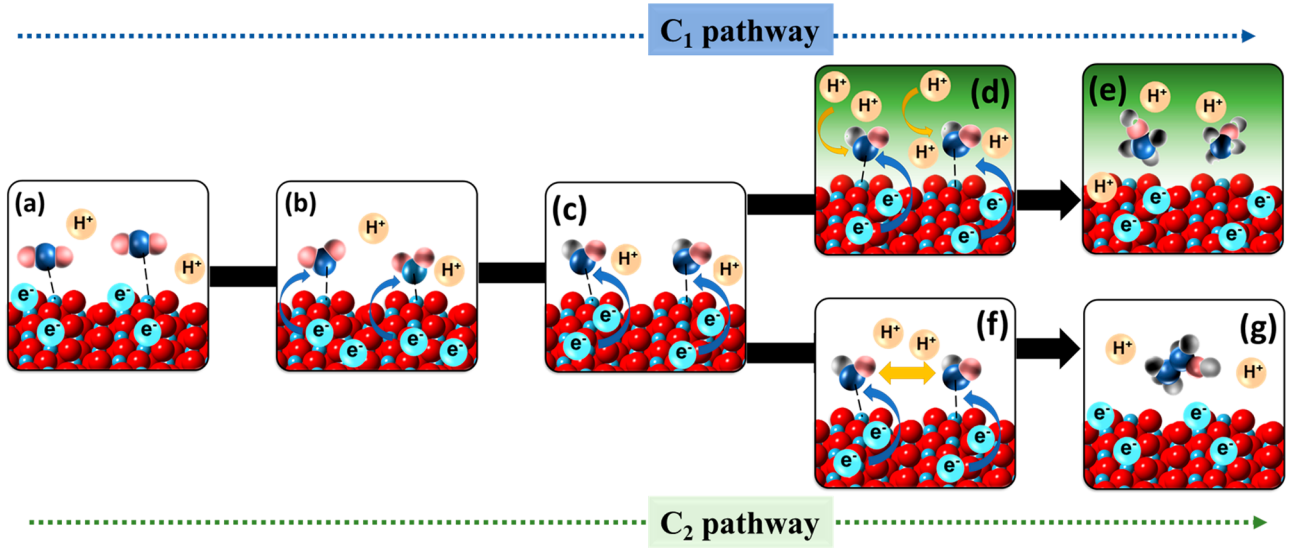

Note that the decrease of the ΔE_0 value in XAFS analysis means reduction of Ti ions, reported by previous studies,[34,35] and the Ti^{3+} state with ΔE_0 = 20.19 eV (Figure 3c) means that surface-exposed Ti atoms of the dark cathodes participate in CO_2 reduction with the following process

$$Ti^{4+} + e^- \rightarrow Ti^{3+}$$

$$Ti^{3+} + CO_2 \rightarrow Ti^{4+} + CO_2^{\bullet -}$$

The coordination binding of CO_2 to the Ti^{3+} on an oxygen vacancy site can allow charge transfer from the TiO_2 electrode surface to the adsorbed CO_2 molecule. Compared with the existence of Ti^{4+} on a Ti atom, the Ti^{3+} state should act as a catalytic active site for PEC CO_2 reduction.

More direct evidence that Ti atoms in dark cathodes participate in CO_2RR was identified in in situ EXAFS analysis. In pristine anatase TiO_2 (tetragonal, $I4_1/amd$ space group), the Ti−O interatomic distance in the TiO_2 dark cathode was 1.87 Å, which is consistent with the Ti−O bond length of pristine anatase TiO_2. The Ti−O bond length decreased to 1.81 Å due to CO_2 adsorption on the electrode surface and finally changed to 1.77 Å when a bias potential under 1 sun illumination was applied for PEC CO_2RR (Figure 3d). In comparison, in the Nf-TiO_2 dark cathode, the Ti−O interatomic distance changed from 1.65 to 1.62 Å for purged CO_2 and to 1.59 Å when a bias potential under 1 sun illumination was applied for PEC CO_2RR (Figure 3e). The tendency of the decreased interatomic distance between Ti and O atoms on the TiO_2 surface indicates that the exposed Ti atoms in TiO_2 crystals have chemically bonded with the CO_2 molecule.[36]

The Ti−C bond between the TiO_2 surface and CO_2 molecules is shorter than the Ti−O bond on the original TiO_2 lattice, which is calculated from first-shell computational results and fitted in Figure S5. The shorter Ti−O interatomic distance on Nf-TiO_2 rather than the TiO_2 cathode is derived from a surface-coated Nafion layer due to Ti−C bonding formed by surface-attached carbon atoms from the Nafion layer. It contributes to the shorter atomic distance derived from the higher electronegativity of surface-attached carbon atoms compared to surface-exposed Ti atoms.

The quantitative analysis on the CO_2 radical anion ($CO_2^{\bullet -}$) between dark cathodes was compared by in situ EPR analysis in Figure 4a. The CO_2 radical anion captured by *N-tert*-butyl-α-phenylnitrone (PBN) and the CO_2 radical−PBN complex is detected by in situ EPR (Figure S6a). The CO_2 radical−PBN complex was detected with a g value of 2.006 with a splitting constant of 45 G (Figure S6b).[37] The EPR signal was negligibly detected when N_2 was purged on both TiO_2 and Nf-TiO_2 dark cathodes. It is worth noting that the unpaired electrons were well detected during PEC CO_2RR on the TiO_2 dark cathode (Figure 4b).

Under PEC CO_2RR with a Nf-TiO_2 dark cathode, the unpaired electron of the CO_2 radical−PBN complex appeared (Figure 4c). It indicates that CO_2 had been reduced to $CO_2^{\bullet -}$ through the first electron transfer reaction from the Nf-TiO_2 dark cathode. Together with the NMR spectrum, it is concluded that transferred electrons from the Nf-TiO_2 dark cathode to CO_2 molecules trigger the formation of CO_2 radical anions, which take further steps to evolve methanol as a unique liquid product under sufficient proton conditions of the catholyte around the cathode, facilitated by a Nafion layer on the dark cathode. Although there is no semiconductor able to provide enough potential for single electron transfer to form a CO_2 radical naturally,[38] an applied external potential in the PEC CO_2RR system enables single electron transfer to the CO_2 molecule; as a result, a CO_2 radical ion is formed and further reduction steps to alcohol proceed.[39] Quantitatively, EPR spectra were collected more clearly on the TiO_2 dark cathode rather than the Nf-TiO_2 dark cathode during PEC CO_2RR because of the high CO_2 radical concentration in the catholyte of the TiO_2 dark cathode, which resulted in a higher CO_2RR product concentration, even if it had lower product selectivity, in the TiO_2 dark cathode.

On the basis of in situ XAFS and in situ ESR monitoring, the C_1 and C_2 alcohol evolution mechanism by TiO_2 and Nf-TiO_2 dark cathodes during PEC CO_2RR is proposed by Scheme 1. Initially, a photon-induced electron from the photoanode is charged on the dark cathode, and Ti^{4+} at the TiO_2 surface is changed to a reactive Ti^{3+} site, which facilitates the absorption of a CO_2 molecule on a dark cathode during PEC CO_2RR

DOI: 10.1021/acsenergylett.9b00927
ACS Energy Lett. 2019, 4, 1549−1555

(Scheme 1a). Then, the accumulated electrons on the surface of the dark cathode are transferred to surface-adsorbed CO_2 and result in the formation of $CO_2^{\bullet-}$ (Scheme 1b). The proton transfer step is accomplished from the catholyte to CO_2 radical anion (Scheme 1c) following the proton-assisted electron transfer step for C_1 and C_2 alcohols. In the process of the proton-assisted electron transfer reaction, the reaction rate depends on the proton density in the catholyte around the cathode surface because mass transport of the proton is kinetically unfavorable compared to electron transfer. In this manner, CO_2RR products can be controlled by the proton transfer rate, is which related to proton concentration in the catholyte. The relative deficiency of the proton on the cathode surface drives CO_2 radical anions to dimerize each other and results in the formation of C_2 alcohol (ethanol). Especially striking, note that the Nafion functional layer acts as a facilitator for plentiful proton density on the catholyte around the Nf-TiO_2 dark cathode surface.[40] Abundant proton in the catholyte surface accelerates a kinetically faster transfer rate and results in the formation of C_1 alcohol by preventing dimerization between CO_2 radical anions (Scheme 1d). In comparison to the mixture of C_1 and C_2 alcohol that evolved as the liquid product by PEC CO_2 reduction using the TiO_2 dark cathode (Scheme 1g), the Nf-TiO_2 dark cathode is selectively driven to evolve only C_1 alcohol (methanol) by PEC CO_2RR (Scheme 1e).

In summary, CO_2 valorization into liquid solar fuel requires sequential transfer of multielectrons to a surface-adsorbed CO_2 molecule from the cathode, accompanied by a proton transfer process to a surface-adsorbed CO_2 molecule from the electrolyte, where oxidation and reduction of the CO_2 radical anion occur simultaneously as a one-pot reaction. In this point of view, the lower proton concentration and slow mass transport kinetics of protons in the catholyte inhibit liquid fuel production on the cathode, producing proton-free products as a CO_2 reduction product such as CO. The Nafion coating on the cathode facilitate faster proton transport and high proton concentration at the catholyte, enhancing the efficiency and product selectivity of the PEC CO_2 reduction system. The present work demonstrates the introduction of a dark cathode for PEC CO_2RR, which is composed of a (040)-BVO photoanode and Nf-TiO_2 dark cathode in a TEAP-ACN electrolyte. Given in situ XAFS and in situ ESR monitoring, the Nf-TiO_2 dark cathode provides abundant protons and results in the formation of C_1 alcohol, methanol, as the unique liquid product evolved by PEC CO_2RR, while the absence of a Nafion layer in the dark cathode drives the formation of a mixture of C_1 and C_2 alcohol by the dimerization path. This work suggests that the role of the Nafion functional layer in the path of PEC CO_2 valorization is to achieve selectivity of alcohol evolved with a higher density of the proton.

■ ASSOCIATED CONTENT

Supporting Information

The Supporting Information is available free of charge on the ACS Publications website at DOI: 10.1021/acsenergylett.9b00927.

Experimental section, XRD patterns, reaction system scheme, NMR spectra, computational calculation, and fitting results and EPR results (PDF)

■ AUTHOR INFORMATION

Corresponding Author

*E-mail: yskang@sogang.ac.kr.

ORCID

Chang Woo Kim: 0000-0001-5821-0041
Hyun Gil Cha: 0000-0002-1228-4464
Wen-Bin Cai: 0000-0003-0500-4791
Young Soo Kang: 0000-0001-5746-8171

Author Contributions

†M.J.K. and C.W.K. contributed equally.

Notes

The authors declare no competing financial interest.

■ ACKNOWLEDGMENTS

This work was supported financially by the Korea Center for Artificial Photosynthesis (KCAP) located at Sogang University (2016M1A2A2947942), which is funded by the Minister of Science, ICT, and Future Planning (MSIP) through the National Research Foundation of Korea and the Brain Korea 21 Plus Project 2018. We also thank Dr. Min Gyu Kim, manager of the 10C beamline at PAL, for helping with XAFS measurements. H.G. Cha thanks to Korea Research Institute of Chemical Technology (KRICT) core project for helping with GC-MS measurements.

■ REFERENCES

(1) Nayak, P. K.; Mahesh, S.; Snaith, H. J.; Cahen, D. Photovoltaic solar cell technologies: analysing the state of the art. *Nat. Rev. Mater.* **2019**, *4* (4), 269−285.

(2) Cha, H. G.; Choi, K.-S. Combined biomass valorization and hydrogen production in a photoelectrochemical cell. *Nat. Chem.* **2015**, *7*, 328.

(3) Kim, D.; Sakimoto, K. K.; Hong, D.; Yang, P. Artificial Photosynthesis for Sustainable Fuel and Chemical Production. *Angew. Chem., Int. Ed.* **2015**, *54* (11), 3259−3266.

(4) Bonke, S. A.; Wiechen, M.; MacFarlane, D. R.; Spiccia, L. Renewable fuels from concentrated solar power: towards practical artificial photosynthesis. *Energy Environ. Sci.* **2015**, *8* (9), 2791−2796.

(5) Su, J.; Vayssieres, L. A Place in the Sun for Artificial Photosynthesis? *ACS Energy Lett.* **2016**, *1* (1), 121−135.

(6) Sun, L.; Hammarstrom, L.; Akermark, B.; Styring, S. Towards artificial photosynthesis: ruthenium-manganese chemistry for energy production. *Chem. Soc. Rev.* **2001**, *30* (1), 36−49.

(7) Graetzel, M. Artificial photosynthesis: water cleavage into hydrogen and oxygen by visible light. *Acc. Chem. Res.* **1981**, *14* (12), 376−384.

(8) Hisatomi, T.; Domen, K. Reaction systems for solar hydrogen production via water splitting with particulate semiconductor photocatalysts. *Nat. Catal.* **2019**, *2*, 387−399.

(9) Mazloomi, K.; Gomes, C. Hydrogen as an energy carrier: Prospects and challenges. *Renewable Sustainable Energy Rev.* **2012**, *16* (5), 3024−3033.

(10) Momirlan, M.; Veziroglu, T. N. Current status of hydrogen energy. *Renewable Sustainable Energy Rev.* **2002**, *6* (1), 141−179.

(11) Ran, J.; Jaroniec, M.; Qiao, S.-Z. Cocatalysts in Semiconductor-based Photocatalytic CO_2 Reduction: Achievements, Challenges, and Opportunities. *Adv. Mater.* **2018**, *30* (7), 1704649.

(12) Tackett, B. M.; Gomez, E.; Chen, J. G. Net reduction of CO_2 via its thermocatalytic and electrocatalytic transformation reactions in standard and hybrid processes. *Nat. Catal.* **2019**, *2*, 381−386.

(13) Stolarczyk, J. K.; Bhattacharyya, S.; Polavarapu, L.; Feldmann, J. Challenges and Prospects in Solar Water Splitting and CO_2 Reduction with Inorganic and Hybrid Nanostructures. *ACS Catal.* **2018**, *8* (4), 3602−3635.

DOI: 10.1021/acsenergylett.9b00927
ACS Energy Lett. 2019, 4, 1549−1555

(14) Liu, S.; Cuty Clemente, E. R.; Hu, T.; Wei, Y. Study of spark ignition engine fueled with methanol/gasoline fuel blends. *Appl. Therm. Eng.* **2007**, *27* (11), 1904−1910.
(15) Di Noto, V.; Negro, E.; Gliubizzi, R.; Lavina, S.; Pace, G.; Gross, S.; Maccato, C. A Pt−Fe Carbon Nitride Nano-electrocatalyst for Polymer Electrolyte Membrane Fuel Cells and Direct-Methanol Fuel Cells: Synthesis, Characterization, and Electrochemical Studies. *Adv. Funct. Mater.* **2007**, *17* (17), 3626−3638.
(16) Liu, M.; Lu, Y.; Chen, W. PdAg Nanorings Supported on Graphene Nanosheets: Highly Methanol-Tolerant Cathode Electrocatalyst for Alkaline Fuel Cells. *Adv. Funct. Mater.* **2013**, *23* (10), 1289−1296.
(17) Zhou, X.; Xiang, C. Comparative Analysis of Solar-to-Fuel Conversion Efficiency: A Direct, One-Step Electrochemical CO_2 Reduction Reactor versus a Two-Step, Cascade Electrochemical CO_2 Reduction Reactor. *ACS Energy Lett.* **2018**, *3* (8), 1892−1897.
(18) Zhu, W.; Zhang, L.; Yang, P.; Hu, C.; Dong, H.; Zhao, Z.-J.; Mu, R.; Gong, J. Formation of Enriched Vacancies for Enhanced CO_2 Electrocatalytic Reduction over AuCu Alloys. *ACS Energy Lett.* **2018**, *3* (9), 2144−2149.
(19) Wang, Y.; Tian, Y.; Yan, L.; Su, Z. DFT Study on Sulfur-Doped g-C_3N_4 Nanosheets as a Photocatalyst for CO_2 Reduction Reaction. *J. Phys. Chem. C* **2018**, *122* (14), 7712−7719.
(20) Kumari, N.; Haider, M. A.; Agarwal, M.; Sinha, N.; Basu, S. Role of Reduced CeO_2(110) Surface for CO_2 Reduction to CO and Methanol. *J. Phys. Chem. C* **2016**, *120* (30), 16626−16635.
(21) Raciti, D.; Wang, C. Recent Advances in CO_2 Reduction Electrocatalysis on Copper. *ACS Energy Lett.* **2018**, *3* (7), 1545−1556.
(22) Tomita, Y.; Teruya, S.; Koga, O.; Hori, Y. Electrochemical Reduction of Carbon Dioxide at a Platinum Electrode in Acetonitrile-Water Mixtures. *J. Electrochem. Soc.* **2000**, *147* (11), 4164−4167.
(23) Paddison, S. J.; Paul, R. The nature of proton transport in fully hydrated Nafion®. *Phys. Chem. Chem. Phys.* **2002**, *4* (7), 1158−1163.
(24) Kim, T. W.; Choi, K.-S. Nanoporous $BiVO_4$ Photoanodes with Dual-Layer Oxygen Evolution Catalysts for Solar Water Splitting. *Science* **2014**, *343* (6174), 990−994.
(25) Kim, C. W.; Son, Y. S.; Kang, M. J.; Kim, D. Y.; Kang, Y. S. (040)-Crystal Facet Engineering of $BiVO_4$ Plate Photoanodes for Solar Fuel Production. *Adv. Ener. Mater.* **2016**, *6* (4), 1501754.
(26) Ji, Y.; Luo, Y. New Mechanism for Photocatalytic Reduction of CO_2 on the Anatase TiO_2(101) Surface: The Essential Role of Oxygen Vacancy. *J. Am. Chem. Soc.* **2016**, *138* (49), 15896−15902.
(27) Mendieta-Reyes, N. E.; Díaz-García, A. K.; Gómez, R. Simultaneous Electrocatalytic CO_2 Reduction and Enhanced Electrochromic Effect at WO_3 Nanostructured Electrodes in Acetonitrile. *ACS Catal.* **2018**, *8* (3), 1903−1912.
(28) Ramesha, G. K.; Brennecke, J. F.; Kamat, P. V. Origin of Catalytic Effect in the Reduction of CO_2 at Nanostructured TiO_2 Films. *ACS Catal.* **2014**, *4* (9), 3249−3254.
(29) Chang, X.; Wang, T.; Zhang, P.; Wei, Y.; Zhao, J.; Gong, J. Stable Aqueous Photoelectrochemical CO_2 Reduction by a Cu_2O Dark Cathode with Improved Selectivity for Carbonaceous Products. *Angew. Chem., Int. Ed.* **2016**, *55* (31), 8840−8845.
(30) Saravanakumar, D.; Song, J.; Lee, S.; Hur, N. H.; Shin, W. Electrocatalytic Conversion of Carbon Dioxide and Nitrate Ions to Urea by a Titania−Nafion Composite Electrode. *ChemSusChem* **2017**, *10* (20), 3999−4003.
(31) Koca, A. Hydrogen evolution reaction on glassy carbon electrode modified with titanyl phthalocyanines. *Int. J. Hydrogen Energy* **2009**, *34* (5), 2107−2112.
(32) Matsubara, Y. Standard Electrode Potentials for the Reduction of CO_2 to CO in Acetonitrile−Water Mixtures Determined Using a Generalized Method for Proton-Coupled Electron-Transfer Reactions. *ACS Energy Lett.* **2017**, *2* (8), 1886−1891.
(33) Hanselman, S.; Koper, M. T. M.; Calle-Vallejo, F. Computational Comparison of Late Transition Metal (100) Surfaces for the Electrocatalytic Reduction of CO to C_2 Species. *ACS Energy Lett.* **2018**, *3* (5), 1062−1067.
(34) Kanchanawarin, J.; Limphirat, W.; Promchana, P.; Sooknoi, T.; Maluangnont, T.; Simalaotao, K.; Boonchun, A.; Reunchan, P.; Limpijumnong, S.; T-Thienprasert, J. Local structure of stoichiometric and oxygen-deficient A2Ti6O13 (A = Li, Na, and K) studied by X-ray absorption spectroscopy and first-principles calculations. *J. Appl. Phys.* **2018**, *124* (15), 155101.
(35) Wan, J.; Chen, W.; Jia, C.; Zheng, L.; Dong, J.; Zheng, X.; Wang, Y.; Yan, W.; Chen, C.; Peng, Q.; Wang, D.; Li, Y. Defect Effects on TiO_2 Nanosheets: Stabilizing Single Atomic Site Au and Promoting Catalytic Properties. *Adv. Mater.* **2018**, *30* (11), 1705369.
(36) Sohn, Y.; Huang, W.; Taghipour, F. Recent progress and perspectives in the photocatalytic CO_2 reduction of Ti-oxide-based nanomaterials. *Appl. Surf. Sci.* **2017**, *396*, 1696−1711.
(37) LaCagnin, L. B.; Connor, H. D.; Mason, R. P.; Thurman, R. G. The carbon dioxide anion radical adduct in the perfused rat liver: relationship to halocarbon-induced toxicity. *Mol. Pharmacol.* **1988**, *33* (3), 351−357.
(38) Tran, P. D.; Wong, L. H.; Barber, J.; Loo, J. S. C. Recent advances in hybrid photocatalysts for solar fuel production. *Energy Environ. Sci.* **2012**, *5* (3), 5902−5918.
(39) Kočí, K.; Obalová, L.; Šolcová, O. Kinetic study of photocatalytic reduction of CO_2 over TIO_2. *Chem. Process Eng.* **2010**, *31*, 395−407.
(40) Kim, W.; Seok, T.; Choi, W. Nafion layer-enhanced photosynthetic conversion of CO_2 into hydrocarbons on TiO_2 nanoparticles. *Energy Environ. Sci.* **2012**, *5* (3), 6066−6070.

DOI: 10.1021/acsenergylett.9b00927
ACS Energy Lett. 2019, 4, 1549−1555